Oriented Films from Recycled Poly(ethylene terephthalate)/Recycled High-Density Polyethylene Compatibilized Blends

J. Morawiec,[1] N. P. Krasnikova,[1,*] A. Galeski,[1] M. Pracella[2]

[1]*Centre of Molecular and Macromolecular Studies, Polish Academy of Sciences, Lodz, Poland*
[2]*Centre of Studies on Multiphase and Biocompatible Macromolecular Materials, National Research Council, Pisa, 56100, Italy*

Received 25 April 2001; accepted 7 February 2002

ABSTRACT: The process for the compatibilized blending of recycled poly(ethylene terephthalate) and recycled high-density polyethylene with ethylene/glycidyl methacrylate copolymer was enlarged to the scale of a pilot plant. The addition of a compatibilizer effectively reduced the size of dispersed inclusions with better bonding to the matrix. The optimum contents of the compatibilizer were found to be around 4 pph. The extrusion and orientation of films from the blend were developed on an industrial scale, and the structure and properties of the obtained films were characterized. The crystalline phase of poly(ethylene terephthalate) in oriented films assumed a strong texture resulting from the plane-strain state of the deformation of the films on the industrial machinery. The origin of the texture was mostly strain-induced crystallization. The chain segments in the amorphous phase were oriented along the machine direction, but there was significant anisotropy of the chain packing in the amorphous phase in the plane perpendicular to the drawing direction, the pseudohexagonal packing of chain fragments being in register over the whole film. Such a texture of an oriented amorphous phase of poly(ethylene terephthalate) is reported here for the first time. The nonoriented and oriented films obtained with the industrial machinery showed good mechanical properties, with strengths up to 120 MPa and elongations to break of 40%. © 2002 Wiley Periodicals, Inc. J Appl Polym Sci 86: 1486–1496, 2002

Key words: blends; compatibilization; films; orientation; polyethylene (PE); recycling

INTRODUCTION

Success in recycling relies very much on the chemistry of the polymer involved and on the purity of the scrap. Polyethylene (PE), polypropylene, poly(ethylene terephthalate) (PET), poly(vinyl chloride), and polystyrene are the most common scrap plastics. In the total volume of waste in Europe, plastics are 65% polyolefins.[1] In the countries of Central Europe, the percentage of polyolefins in waste is not different. PET constitutes 5 wt % of the plastic waste in Europe.[1] In Poland, 1.2 billion PET bottles in 2000 were used for soft drinks, and the amount is increased by 25% per year.[2] In principle, all of it could be recovered and recycled. It is estimated that in Central and Eastern Europe, the consumption of PET for packaging will grow 14% per year during the next 5 years, reaching a total of 800,000 tons in 2005.

At present, the automated processes for the segregation of scrap material according to the polymer type have not been 100% correct; usually, a number of different polymers are collected.

The successful recycling of PET relies on the process that ensures the separation of PET bottles from other scrap polymers, and then the bottles are processed by careful washing, cutting, and grain classification by size.[3,4] The process consists of no regranulation step, thereby avoiding additional degradation. Thorough drying followed by melt filtering and the addition of appropriate antioxidants leads to high-quality extruded products from recycled PET (R-PET). This procedure is costly and not 100% efficient. Therefore, scrap polymers usually have poor mechanical properties, which are the result of degradation during processing and the presence of large amounts of polymeric and nonpolymeric inclusions. Because R-PET contains a mixture of polyolefins, whereas polyolefin recyclates are usually mixtures also containing PET, blending seems to be a good way of recycling without careful segregation. The crucial problem is that, when polymers are blended, many important properties are severely depressed because of the incompatibility of

Correspondence to: A. Galeski (andgal@bilbo.cbmm.lodz.pl).
**Permanent address:* Institute of Petrochemical Synthesis, Russian Academy of Sciences, Moscow, Russia.
Contract grant sponsor: EU INCO-Copernicus; contract grant number: IC15 CT96 0731.
Contract grant sponsor: Centre of Molecular and Macromolecular Studies (Polish Academy of Sciences).

components. The reprocessing of commingled waste plastics usually leads to poor physical properties of the product. The compatibilization of polymer components provides a chance to avoid the requirement of complete segregation of waste plastic before recycling. Compatibilization is often expensive in comparison with the value of raw polymers. However, there are some polymer systems for which the compatibilization may be simple enough and not expensive. Then, the end product is higher in grade and value, which could make the recycling economically profitable.

The compatibility of R-PET and recycled high-density polyethylene (R-HDPE) can be enhanced in several ways, including both reactive and nonreactive processes.[5,6] The reactive compatibilization of model blends of PET and HDPE has been examined in several articles and reviews. Blends of PET/HDPE have been compatibilized by the addition of maleic anhydrate grafted polyolefins,[7,8] styrene–ethylene/butylene–styrene (SEBS) block copolymers and maleated SEBS (SEBS-*g*-MA) copolymers,[9] ethylene/acrylic acid copolymers, ethylene/glycidyl methacrylate (EGMA) copolymers, and ethylene/ethyl acrylate/glycidyl methacrylate terpolymers.[4,10–14]

The compatibilization of commingled scraps of PET and HDPE for upgrading their properties was of little concern in the past. Xanthos et al.[15] studied the compatibilization of commingled postconsumer plastics containing various polymers, including PET and HDPE, via melt blending with SEBS, SEBS-*g*-MA, and maleated ethylene–propylene rubber (EPR) rubber. The reactive compatibilization of PET and PE recyclates, which were derived from beverage bottles and plastic waste, was carried out by the melt radical grafting of R-HDPE with glycidyl methacrylate monomer.[16] In another article in this issue, we discuss the compatibilization of R-PET/R-HDPE blends with several compatibilizers, including reactive EGMA and SEBS-MA.[17]

The best results for blending R-PET and recycled PE (R-PE) were obtained for a random EGMA copolymer when the compatibilization was performed in a corotating twin-screw extruder. The blending process was optimized for the concentration of the compatibilizer and the processing conditions. For the average concentration of 25 wt % R-PE in R-PET, the addition of 4 pph EGMA gave the best tensile and impact properties. The properties of the optimized blends containing 75 wt % R-PET, 25 wt % R-PE, and 4 pph EGMA allowed for the smooth extrusion of films on the laboratory scale.

The goal of this work is to develop the processes of compatibilization, film extrusion, and film orientation on an industrial scale and to characterize the structure, texture, and properties of the obtained films.

EXPERIMENTAL

Materials

Recyclates of PET and polyolefins were acquired from producers in Italy: R-PET (400 kg) from postconsumer beverage bottles (Rilat, from Replastic Co., Milano, Italy) and PE (R-HDPE; 400 kg) from bottles and containers for household liquids (Rilae, from Replastic Co.). R-PET had a melt-flow index of 25.3 g/10 min (2.16 kg at 265°C) and an intrinsic viscosity of 0.757 dL/g as measured with Ubbelohde viscometry at 25°C (a mixture of phenol and 1,1,2,2-tetrachloroethane in a 6/4 w/w ratio was used as a solvent). It contained 0.01% poly(vinyl chloride) and 0.2% PET with glue. Representative samples (5 kg) were homogenized by extrusion and characterized by various techniques. Detailed studies of the compositions and properties are described elsewhere.[17]

R-PE had a melt-flow index of 0.8 g/10 min (2.16 kg at 265°C) and contained such impurities as 3.9 wt % polypropylene, 1.5% low-density polyethylene (LDPE), and 2.2 wt % pigments and mineral fillers. The oxidation induction time (according to European Norm EN 738 at 200°C with an oxygen flow of 50 mL/min) was 3.9 min.

The EGMA copolymer Lotader AX8840 (Elf Atochem, Italy), containing 8 wt % active glycidyl methacrylate, was used as a compatibilizer.

Blending

A twin-screw corotating extruder (with nonintermeshing, one-dimensional segmented screws and a half-sectioned cylinder, $D = 25$ mm and $L/D = 33$, assembled to have two venting zones) was used for blending. The temperatures of the heating zones were set at 250, 260, and 270°C, with the head at 270°C. The screw rotation speed was set at 88 rpm, which allowed for a 7-min residence time. An R-PET/R-HDPE blend with 75% R-PET, 25% R-HDPE, and 4 pph EGMA was prepared in a large amount. Extruded threads 2 mm in diameter were cooled with blowing dry air, immediately pelletized, and protected from moisture take-up by being sealed in double-layer PE–paper bags. Later, the blend was used for film extrusion on an industrial scale at Terplast Co. (Lodz, Poland).

Film extrusion and orientation

Film extrusion was performed on an extrusion line consisting of an extruder ($D = 60$ mm, $L/D = 25$) equipped with a slot film die 900 mm wide. The temperatures of the five heating zones of the extruder were set at 130, 250, 260, 275, and 285°C, and the temperature of the die was 275°C. The temperature of the chill roll was maintained at 78°C. The screw rotation speed was set to 38 rpm, and the yield of extru-

sion was 25 kg/h. The speed of the chill roll was set at 2.3 m/min. The air knife ensured good contact of the extruded film with the chill roll. The extrusion line was also equipped with a film orientation unit consisting of a row of eight rolls heated slow to fast. The temperature of the rolls was set at 80°C. First, the extruder was cleaned by the extrusion of 50 kg of LDPE, and then the extruded material was changed into a 72.12%/24.04%/3,84% R-PET/R-HDPE/EGMA blend prepared before extrusion and kept sealed in moisture-tight bags. The unoriented film was extruded for approximately 1 h. Then, the film orientation unit was put in operation and set to produce oriented films at six various orientation ratios: 1.5, 2.0, 2.5, 3.0, 3.5, and 4.0.

Properties and structure characterization

The mechanical properties of the films were studied with an Instron tensile testing machine model 1014 (Instron Corp., High Wycomb, UK) at 23°C. Oar-shaped samples with a 100-mm gauge length and a 20-mm width were stretched at a rate of 50 mm/min. Samples were cut from the films along the machine direction and along the transverse direction.

A T300 scanning electron microscope (Jeol Ltd., Akishima, Tokyo) was use to characterize the dispersion of components and the phase structure of the blend and films. Films were fractured after being submerged in LN_2 for a period of 2–3 min, were allowed to return to room temperature in a low-humidity atmosphere, and were covered with a thin layer of gold by ion sputtering.

The thermal properties of the films were determined with a differential scanning calorimetry (DSC) technique (TA 2100, TA Instruments, New Castle, DE). Samples (12–15 mg) were used in the form of several discs 5 mm in diameter. For thinner films with higher draw ratios, more discs were placed in DSC pans. The heating rate in the DSC apparatus was 10°/min.

Dynamic mechanical properties of the blend and films were measured with a Rheometric Scientific (Epsom, UK) MkIII dynamic mechanical thermal analysis (DMTA) apparatus in a dual-cantilever bending mode with fixed ends. The samples were in the form of a rectangle 18 mm wide and 35 mm long. The sample grip allowed for a 2-mm gauge length and an 18-mm width. The sensing frequency was set at 1 Hz, and the amplitude was set at ± 16 μm. The dynamic mechanical properties were measured from -120 to 200°C at a rate of 2°/min.

Thermal shrinkage was studied at 70, 90, and 110°C for 45 min. Samples (100 mm $\times$ 100 mm) were placed between two 0.1-mm-thick polytetrafluoroethylene (PTFE) films lying flat on a glass plate and were squeezed by a 0.5-mm-thick brass plate being placed at the top. The thickness, length, and width of the films were measured after they cooled to room temperature under the load of the brass plate.

The density of the films and the extruded thread was determined in an aqueous solution of NaCl and $ZnCl_2$ at 23°C by floatation. Before being submerged, the samples were placed in an air-evacuated vacuum flask, and the solution of NaCl and $ZnCl_2$ was poured over the samples with the vacuum preserved.

The orientation of the crystalline phase of PET in oriented tapes was studied by means of X-ray diffraction with pole figures. A wide-angle X-ray scattering system consisting of a computer-controlled pole figure device associated with a wide-angle goniometer coupled to a sealed-tube X-ray generator operating at 30 kV and 30 mA was used in this study. The X-ray beam consisted of Cu Kα radiation filtered by a Ni filter and electronically. For pole figure data acquisition, we used a procedure described earlier. The details of the pole figure determination procedure are described elsewhere.[18]

The following diffraction reflections from the triclinic crystal structure of PET were analyzed for the construction of pole figures: (010), (100), and (−105),[19] which were found in our case at the diffraction angles $2\Theta = 17.1$, 25.1, and 42.2°, respectively. The slit system of the diffractometer was always selected for the measurement of the integral intensity of the appropriate diffraction peak. The necessary corrections for background scattering and sample absorption were introduced to raw data. The pole figure plots were generated by the POD program, a part of the popLA package (Los Alamos National Laboratory, Los Alamos, New Mexico). For every plot, the data were normalized to the random distribution density. In addition to these three integral pole figures for crystallographic peaks, the height pole figure of the amorphous phase was constructed from the diffraction data at $2\Theta = 19.5°$. At this angle, there was a maximum of the amorphous halo of unoriented PET. This region of the diffraction angles was relatively free of crystalline diffraction peaks of PET and PE.

RESULTS

A 75 wt %/25 wt %/4 pph R-PET/R-HDPE/EGMA blend (75 kg) was prepared in a laboratory corotating twin-screw extruder. The extruder residence time was about 5–7 min. The blending extrusion was trouble-free, with a yield of 1 kg of the blend per hour. The surface of the threads was smooth, and the color was gray-green. The density of the threads was 1.25 ± 0.03 g/cm^3, which indicated some degree of crystallinity of PET. The DSC thermogram during heating at a rate of 10°/min is presented in Figure 1. There can be seen a small, wide peak of melting of EGMA at 100°C, a small exothermic peak corresponding to the residual cold crystallization of PET around 123°C overlapped

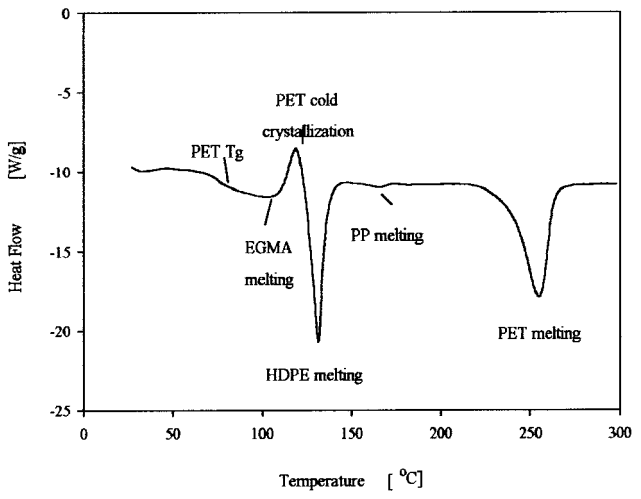

Figure 1 DSC thermogram of an extruded thread of a 75%/25%/4 pph R-PET/R-HDPE/EGMA blend.

and followed by an endothermic peak of melting of HDPE at 131°C, and a small peak corresponding to the melting of isotactic polypropylene impurities; at 254.7°C, PET crystals formed during solidification and formed by cold crystallization during the DSC run melted. The micrograph of the fracture surface (at the LN_2 temperature) of the extruded thread is presented in Figure 2(a). The extruded spaghetti shows a rather homogeneous fracture surface, and phase separation can hardly be seen. This demonstrates the high mixing efficiency of the twin-screw corotating extruder. However, when the film was obtained from the spaghetti by compression molding, the inclusions of R-HDPE appear visible, being a few micrometers in diameter on average. This indicates a rather high intensity of the coalescence of R-HDPE inclusions that occurred during the time needed for compression molding (ca. 4 min at 270°C). The coalescence was intensified by the low viscosity of R-PET in the molten state.

The process of film extrusion on the industrial extruder was flawless; the films were smooth on the side touching the chill roll, nontransparent, and gray-green. The other side of the film was slightly rough, with occasional small heaps rising 0.001–0.005 mm above the film surface. The blobs were sporadic microgels around fillers, pigment particles, or solid impurities present in R-HDPE, as revealed by light microscopy and scanning electron microscopy (SEM). The quality of the surface of the film was worse than that of pure PET and worse than that of a PET/HDPE blend from virgin components.[20] However, the films fulfilled the basic requirements for films for the packaging of technical goods, such as backings of blister packs and thermoformed containers. The smoothness of the side of the film touching the chill roll indicated that the unoriented film could be smooth on both sides if extruded between two smooth chill rolls. The color and nontransparency of the films resulted from pigments and fillers present in R-HDPE rather than from preferential light scattering by R-HDPE inclusions. The thickness of the film varied from 0.22 to 0.28 mm, depending on the speed of the chill roll, but the thickness across the film was uniform, except that at the edges the film was slightly thicker. At a speed of 2.3 m/min, the film thickness stabilized at 0.28 mm. The extrusion was observed for 1 h, and samples were collected. The yield at this speed and film thickness approached 25 kg/h.

An SEM micrograph of a film is shown in Figure 3(a). The inclusions of R-HDPE appeared to be a few micrometers in diameter on average, and some large inclusions, nearly 10 μm in diameter, can be seen. However, the uncovered surface of the inclusions was not smooth, indicating a high level of attachment to the R-PET matrix. The effect can be especially well seen at some distance from the notch, where the fracture occurred at low speed [Fig. 3(b)]. The surfaces of the inclusions were rough, with tufts of highly deformed, undetached, and broken polymeric material. Most likely, EGMA compatibilizer preferentially located at the interface. There was no significant difference in the film morphology in the directions parallel and perpendicular to the extrusion direction.

The orientation step in the film extrusion line was set a various elongation ratios: 1.5, 2.0, 2.5, 3.0, 3.5, and 4.0. The film was solidified on a chill roll and then passed to the system of slow and fast rolls. The orientation was conducted at a temperature near the glass-transition temperature of R-PET (T_g = 78–80°C). R-HDPE inclusions were already crystallized at 78–80°C when the film passed to the stretching unit. The process of orientation was trouble-free; no fracture occurred within 30 min of the extrusion and film orientation for each elongation ratio. The resulting films

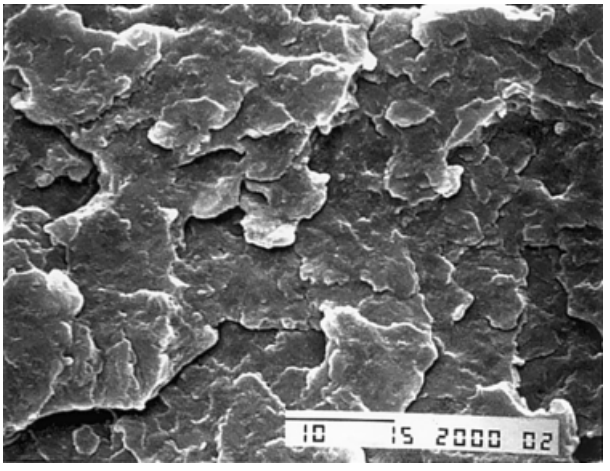

Figure 2 SEM micrograph of the LN_2 fracture surface of an extruded thread of a 75%/25%/4 pph R-PET/R-HDPE/EGMA blend.

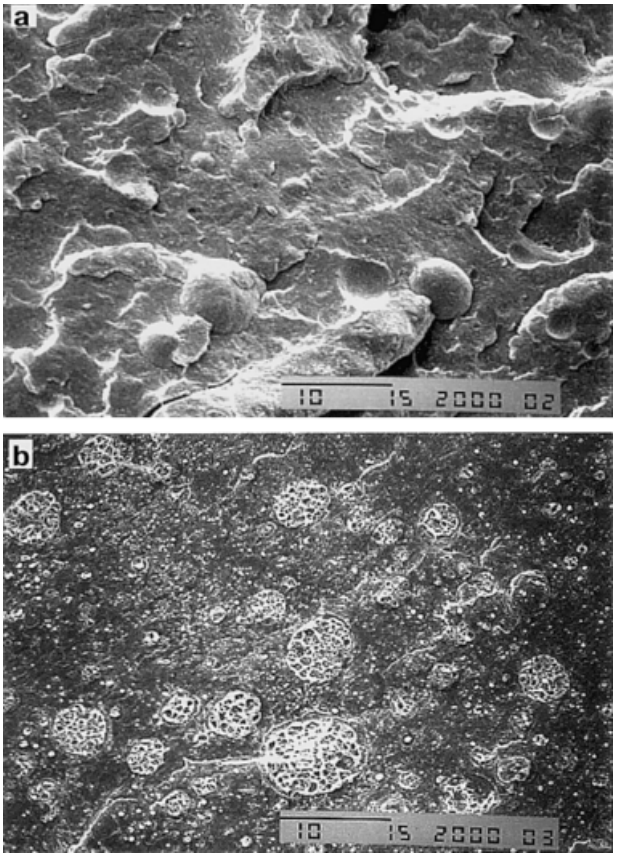

Figure 3 SEM micrographs of the LN_2 fracture surface of a nonoriented extruded film of a 75%/25%/4 pph R-PET/R-HDPE/EGMA blend: (a) near the notch and (b) far from the notch.

varied in thickness; the thicknesses were 0.25, 0.18, 0.16, 0.09, 0.06, and 0.05 mm for elongation ratios of 1.5, 2.0, 2.5, 3.0, 3.5, and 4.0, respectively. The elongation ratio was determined from the distance between ink marks before stretching and after stretching, and the speed of the fast rolls was adjusted accordingly.

Figure 4 SEM micrograph of the surface of an oriented extruded film of a 75%/25%/4 pph R-PET/R-HDPE/EGMA blend. The draw ratio of the film was 3.5, and the surface was exposed by fracturing in LN_2 along the drawing direction.

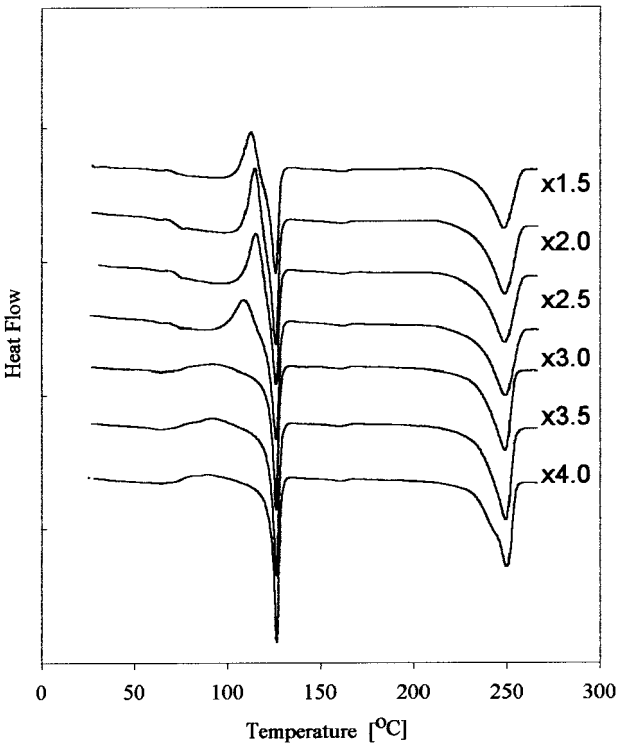

Figure 5 DSC thermograms of unoriented and oriented R-PET/R-HDPE/EGMA films. The draw ratio is depicted on the graph for each sample.

A fine dispersion of R-HDPE inclusions was demonstrated in oriented films by SEM (Fig. 4). R-HDPE inclusions formed elongated, fibrillar structures; for the film stretched to a draw ratio of 3.5, the inclusions were 10–20 μm long and 2–3 μm wide (Fig. 4). Less oriented material was present at the edges of films. Because the HDPE inclusions, which were solidified when the film was deformed, assumed an ellipsoidal shape with a high aspect ratio corresponding to the overall drawing ratio, the stresses were effectively transmitted from the PET matrix to HDPE inclusions through the interface. At poles of these elongated features, only small cavities could be seen, indicating the limited detachment of HDPE from PET in these regions in which the tensile stresses assumed peak values.

The thermal data for oriented films are collected in Figure 5. The cold crystallization of PET was visible in nonoriented films, but it decreased with the increase in the elongation ratio, and for an elongation ratio of 4, it reached the very low level of 5.7 J/g. The peak of cold crystallization moved to lower temperatures as the draw ratio increased, from 112.5°C for unoriented films to 88.5°C for a draw ratio of 4. The peak of cold crystallization was 123°C for extruded threads right after blending. It is evident that the extruded films had

TABLE I
ρ of R-PET/R-HDPE/EGMA Oriented Films Measured by the Floatation Method in an Aqueous Solution of $ZnCl_2$ and NaCl at 25°C

Draw ratio	ρ (g/cm^3)
1	1.195
1.5	1.198
2	1.2
2.5	1.204
3	1.205
3.5	1.208
4	1.21

some degree of orientation that accelerated the cold crystallization of PET. This initial orientation was generated during extrusion through the slit and also by the pulling of the molten film from the orifice onto the chill roll. Oriented films were characterized by a higher crystallinity of the PET phase increasing with an increasing degree of orientation from 24.2 to 36.1%, as we calculated from the DSC data in Figure 5 by subtracting the enthalpy of cold crystallization from the enthalpy of melting. It must be mentioned here that the PE melting partially overlapped with the cold crystallization of PET, and so the crystallinity data were not very certain for samples with low draw ratios. The PET melting temperature increased from 248.7°C for unoriented films to 250.2°C for a draw ratio of 4. T_g values could be determined on the basis of DSC thermograms only for low oriented films; for higher orientation, no significant glass-transition shoulder could be distinguished on the DSC curves because it was adjacent to the PET cold crystallization peak and the melting of EGMA.

The melting temperature of R-HDPE inclusions, about 125–126°C, was lower than that for extruded thread. The lowering of the melting temperature of HDPE inclusions was the result of efficient cooling of the film on the chill roll. The enthalpy of melting could not be precisely determined for samples with low draw ratios from the plots in Figure 5 because the endothermic melting peak overlapped with the exothermic peak of cold crystallization of PET. For higher draw ratios, the PET cold crystallization peak was lower and shifted toward lower temperatures; the enthalpy of HDPE melting was determined around 115–122 J/g ,which corresponds to 39–42% HDPE crystallinity in oriented films.

The density of unoriented and oriented films was determined by a floatation method in an aqueous solution of NaCl and $ZnCl_2$ at 23°C (Table I). The density of the films increased with an increasing draw ratio, from 1.19 to 1.21. However, the calculated density of the films obtained from the densities and crystallinities (as measured by DSC) of the components and the compositions of the films was higher than the measured density. For example, for the film oriented to a draw ratio of 4, the density of the film should be 1.244 g/cm^3 (PET crystallinity = 36%, amorphous phase = 1.335 g/cm^3, crystalline phase = 1.455 g/cm^3; HDPE crystallinity = 42%, amorphous phase = 0.855 g/cm^3, crystalline phase =1.0 g/cm^3; EGMA density = 0.905 g/cm^3), but the measured density did not exceed 1.21 g/cm^3. This indicates the existence of a small fraction of cavities in the oriented films. The cavities were formed at the interfaces of PET and HDPE in pole regions of oriented HDPE inclusions during drawing, as evidenced by SEM examination (see Fig. 4).

Thermal shrinkage was studied at 70, 90, and 110°C over 45 min. The changes in the thickness, the length in the machine direction, and the width in the transverse direction of the films were recorded. The data are collected in Table II. The changes in the width were rather small in comparison with the changes in the thickness and length, not exceeding a few percent. This indicates that the drawing of films occurred under plane-strain conditions, that is, with a fixed width. Significant changes in the thickness and length developed with the annealing of oriented films, less at 70°C and more at 90 and 110°C. The unoriented films showed, however, less shrinkage at 110°C than at 90°C because of the development of cold crystallization, which was faster at this temperature than shrinkage. In the oriented films, the capacity for cold crystallization was lowered as these films crystallized during

TABLE II
Thermal Shrinkage of Extruded and Oriented R-PET/R-HDPE/EGMA Films After 45 min of Annealing at Three Different Temperatures

	Thickness (%)			Length (%)			Width (%)		
Draw ratio	70°C	90°C	110°C	70°C	90°C	110°C	70°C	90°C	110°C
1	0.8	45.8	2.9	−9.7	−35	−3.16	1.7	2	0.12
1.5	10.3	43.2	51	−12.8	−32	−37	2	4	2
2	18.2	64.8	73	−21.8	−41	−43.7	1.5	2	−3
2.6	31.7	71	89.2	−30	−39.7	−41.3	1.5	−2.7	−5.3
3	9	46.7	61.9	−5	−24	−34.7	−2	−3.5	−6.3
3.5	5.7	54.3	72.3	−10.7	−25.8	−28	−2	−3.7	−6
4	9.4	28.1	68.8	−6	−17.2	−23	−2.7	−4.5	−6.3

drawing. The shrinkage (thickness and length) of the oriented films increased as the draw ratio increased up to a draw ratio of 2.5. With a further increase in the draw ratio, the shrinkage decreased. These measurements showed that the orientational crystallization stabilized the shape of the films and strengthened the films above the glass transition of PET.

The texture of oriented PET tapes was studied via X-ray diffraction with the construction of pole figures. Pieces of the films, 2 cm × 2 cm, were used, all oriented vertical to the machine direction. In 2Θ scans, the reflections at 17.1, 25.1, and 42.2° corresponded to (010), (100), and (−105) reflections from the triclinic PET crystals. The triclinic crystallographic form of PET has the following parameters: $a = 4.56$ Å, $b = 5.94$ Å, $c = 10.75$ Å, $\alpha = 98.5°$, $\beta = 118°$, and $\gamma = 112°$.[19] The c axis of the unit cell is connected with macromolecular chain axes, whereas the plane of phenyl rings is nearly perpendicular to the a axis. From X-ray diffraction, it is possible to obtain information about the orientation of phenyl rings and chain axes because the normal to the (100) plane is tilted by approximately 19° with respect to the normal to the phenyl ring plane, whereas the position of the (−105) reflection bears information on the orientation of macromolecular chains because the c axis is tilted by 9.8° with respect to the normal to the (−105) plane. At first approximation, the deviations of (100) and (−105) reflections from the a and c axes, respectively, can be disregarded.[21,22] In addition to these three integral pole figures for crystallographic peaks, the height pole figure of the amorphous phase was constructed from the diffraction data at $2\Theta = 19.5°$. At this angle, there was a maximum of the amorphous halo of unoriented PET. Moreover, this region of the diffraction angles is relatively free of crystalline diffraction peaks. The pole figure for the amorphous halo was constructed in the past for PE and polyamide-6 to gain information about the orientation of the amorphous phase.[23,24] In such cases, the amorphous halo was treated as a (100) reflection from close packing of the amorphous phase. Clustering of these reflections gives information about the orientation of those chain fragments that are in the amorphous state. The orthorhombic PE crystals produce the two most intense diffraction peaks from (110) and (200) planes at 21.6 and 24.0°. These peaks do not overlap with the most significant peaks from triclinic crystals of PET and do not interfere with the maximum of the amorphous halo of PET (at 19.5°).

The pole figures collected for the (100), (010), (−105), and amorphous (100) close-packing reflections for PET crystals in oriented films are presented in Figure 6 for an increasing draw ratio. The pole figures indicate the formation of a texture produced during stretching: macromolecular chains in crystals increasingly oriented along the drawing direction according to the clustering of (−105) normals, being stronger with an increasing draw ratio. Normals to (100) planes weakly clustered in the direction around the normal to the film plane for low draw ratios and became more pronounced when the draw ratio reached 2.5. For higher draw ratios, a new population of crystals appeared that concentrated with (100) normals oriented in the transverse direction. The normals to (010) planes of crystals were concentrated at first in two distinct populations tilted at some acute angles in the equatorial plane with respect to the flat film surface. With an increasing draw ratio, that additional fraction of crystals seen in (100) pole figures was located with (010) normals perpendicular to the film surface. Because the initial unoriented material was nearly amorphous, the origin of the texture was mostly the strain-induced crystallization and to a lesser extent the plastic deformation and rotation of newly formed crystals.

The pole figure for the heights of the amorphous halo (Fig. 6) also indicated a significant orientation of chains in the amorphous phase along the drawing direction. There was a significant trace of anisotropic packing of chains of the amorphous phase in the plane perpendicular to the drawing direction in the form of four distinct clusters at roughly −90, +90, −30, and +30° with respect to the film surface. The orientation of the normals to the (100) close-packing plane suggested that the chain segments in the amorphous phase were oriented along the machine direction. The splitting of the clustering of (100) normals in the equatorial zone into a four-point pattern was apparently caused by the pseudohexagonal packing of chain fragments in the amorphous phase of PET, being in register over the whole sample. Projected onto the pole figure, the six-component orientation function produced four equatorial streaks; this occurred because the 240 and 300° components overlapped with the −30 and +30° components, and the −90 and +90° components were visible alone.

The observation of pseudohexagonal packing of the oriented amorphous phase in PET is new and very important because it resolves the old dispute about how the oriented amorphous phase is arranged. A similar feature for amorphous phase packing was observed previously in PE deformed by plane-strain compression in a channel die.[25] Also, here the main deformation mode was plane strain: the geometry of plane-strain tension was enforced by the lateral friction of the film against the system of stretching rolls (eight rolls).

Only a limited orientation of the already formed PET crystals by their plastic deformation is expected in PET/HDPE drawn films. Crystal orientation with macromolecular chains along the drawing direction prevents the generation of significant shear within possible glide planes and directions that were observed in PET:[26] (100)[001] chain slip, (100)[010] transverse slip, and sluggish (010)[001] chain slip. Probably

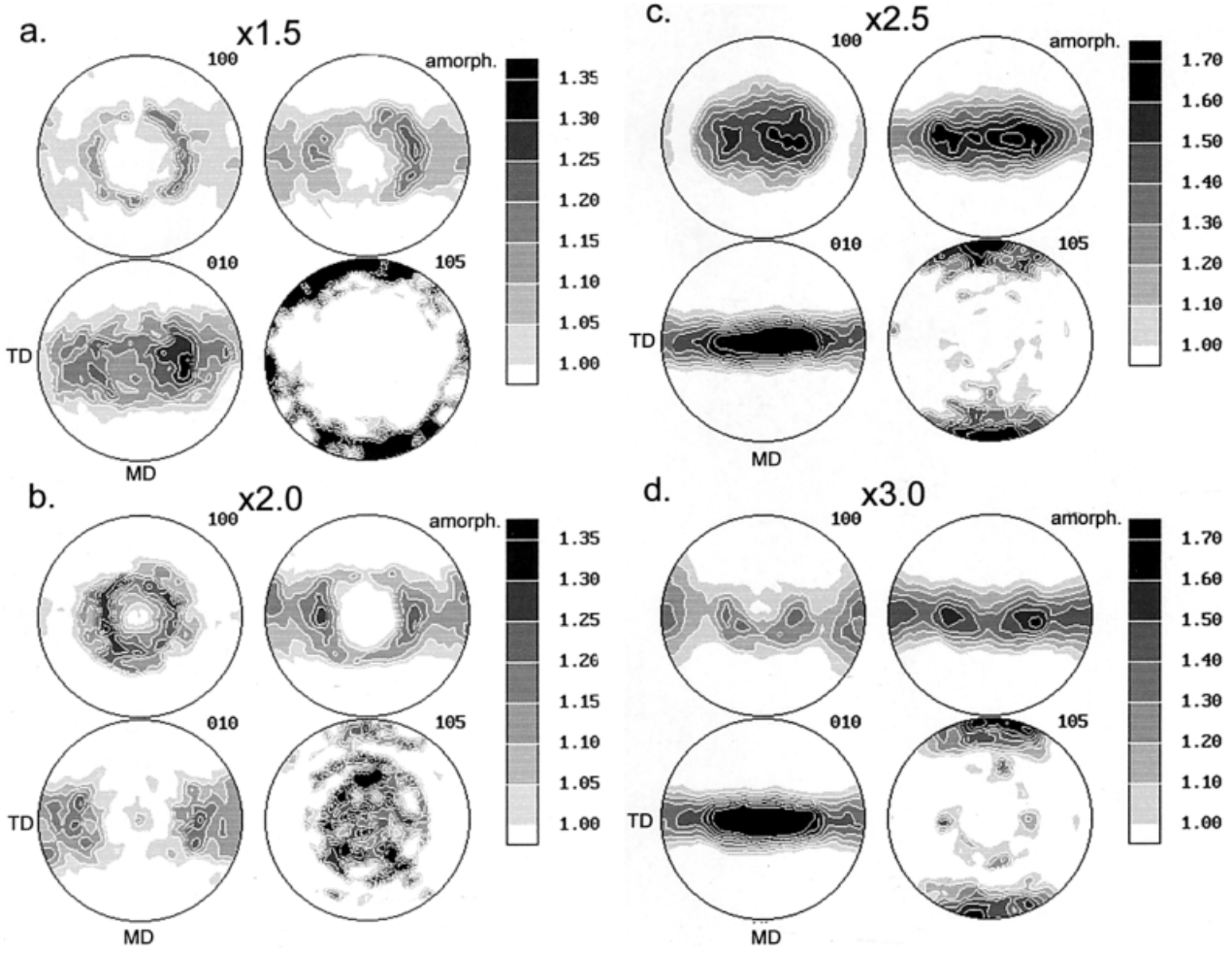

Figure 6 Pole figures of normals to (100), (010), and (−105) planes of triclinic PET crystals for oriented R-PET/R-HDPE/EGMA films. The pole figures for the amorphous halo height are also presented. The draw ratio is given for each sample.

only those less perfectly oriented crystals become beneficially aligned to undergo plastic deformation due to (100)[001] and (100)[010] slips, the (100)[001] chain slip being the easiest.[26]

The dynamic mechanical properties of oriented films were studied via bending in the plane of the film along the machine and transverse directions. The dynamic mechanical imaginary moduli (E'') of the films as a function of temperature are presented in Figure 7(a,b). The most significant transition observed for samples tested along the machine direction was the glass transition at 76–90°C: for a low draw ratio of the films, the glass transition was seen at a lower temperature, whereas for higher draw ratios, T_g approached 90°C. At the temperature above the glass transition for a low draw ratio, E' (not shown here) and E'' drastically dropped because there were too few crystals that could stabilize and strengthen the rubbery amorphous material. Above 110°C, the new crystals were formed by cold crystallization during the DMTA experiment, which stabilized the film structure. With a starting draw ratio of 2.5, the drop in E' and E'' at temperatures beyond the glass transition was not very substantial because these films were stabilized by crystals that were formed during drawing before the DMTA experiments. There was a small shift in the β transition toward a higher temperature with an increasing draw ratio. The β transition became more pronounced with an increasing draw ratio, as seen in Figure 7(a).

Bending in the plane of the film along the transverse direction demonstrated significant differences in DMTA responses of the oriented film [see Fig. 7(b)]. The shift of T_g toward higher temperatures was smaller, from 76°C for the unoriented film to 84°C for the film with the highest draw ratio of 4. This means that the glass transition, which had its origin in the amorphous phase, exhibited anisotropy: the glass transition occurred at different temperatures when the film was bent in different directions. The source of the anisotropy in the glass transition was the anisotropy of the amorphous phase: the pseudohexagonal packing and the orientation of chain segments. Similar anisotropy of the glass transition was noticed by us for

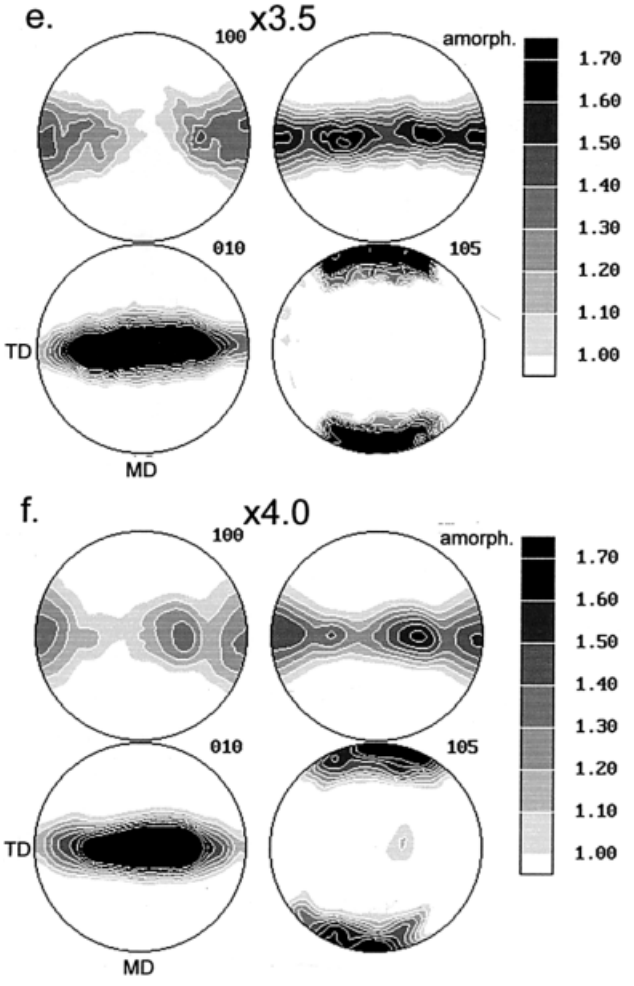

Figure 6 (*Continued from the previous page*)

polypropylene oriented by rolling with side constraints[27] and for superstrong PET tapes obtained by sequential drawing,[28] both means of deformation producing plane strain in the material.

The drop of E' and E'' at a temperature higher than the glass transition was similar to that for testing via bending along the machine direction: below a draw ratio of 2.6, the drop was significant because of the scarcity of crystallinity, whereas for a higher draw ratio, the existing crystals prevented a significant decrease in the moduli. For a low draw ratio, the cold crystallization was seen above 110°C as a peak on the curve of E'' versus temperature.

The shift in the β transition with the increase in the draw ratio and the change in its intensity for samples tested along the transverse direction were similar to those observed for the machine direction [cf. Fig. 7(a,b)].

Mechanical properties of the films were characterized by the stretching of oar-shaped samples at a constant speed at room temperature. Two sets of samples were prepared, one cut out along the machine direction and the other cut along the transverse direction. Typical stress–strain curves for the machine direction are presented in Figure 8(a), and curves for the transverse direction are given in Figure 8(b). The nonoriented film showed good mechanical properties. It deformed plastically, with an elongation to break in the machine direction of 250% and a yield stress at 32–34 MPa; in the transverse direction, the yield stress was at a similar level, whereas the elongation varied widely from 50 to 250%. The orientation of the films reduced the capacity for further large deformation. However, even a film with an orientation of 3.5 was capable of deforming 60% further or even more. The

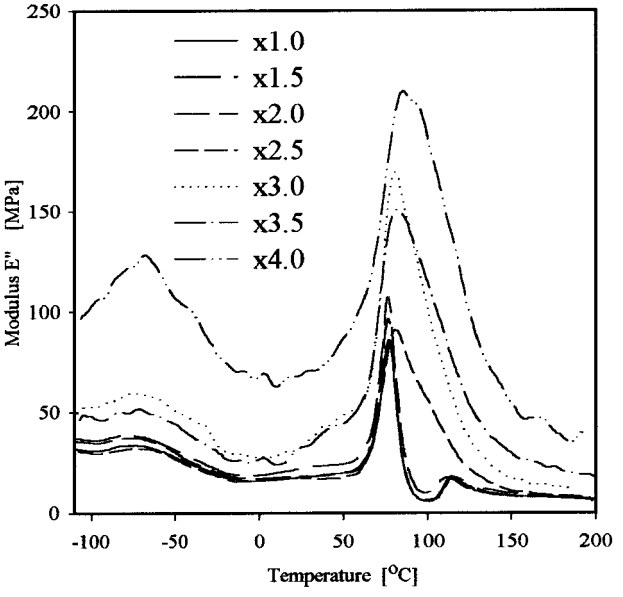

(a)

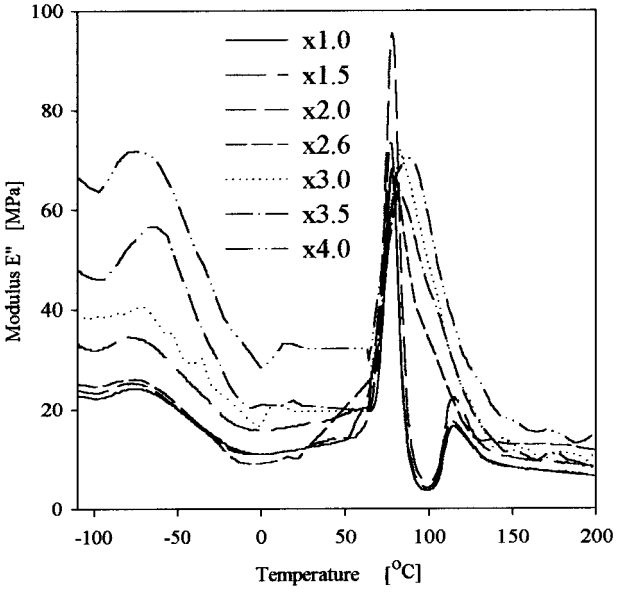

(b)

Figure 7 E'' for nonoriented and oriented films of a 75%/25%/4 pph R-PET/R-HDPE/EGMA blend tested along (a) the machine direction and (b) the transverse direction.

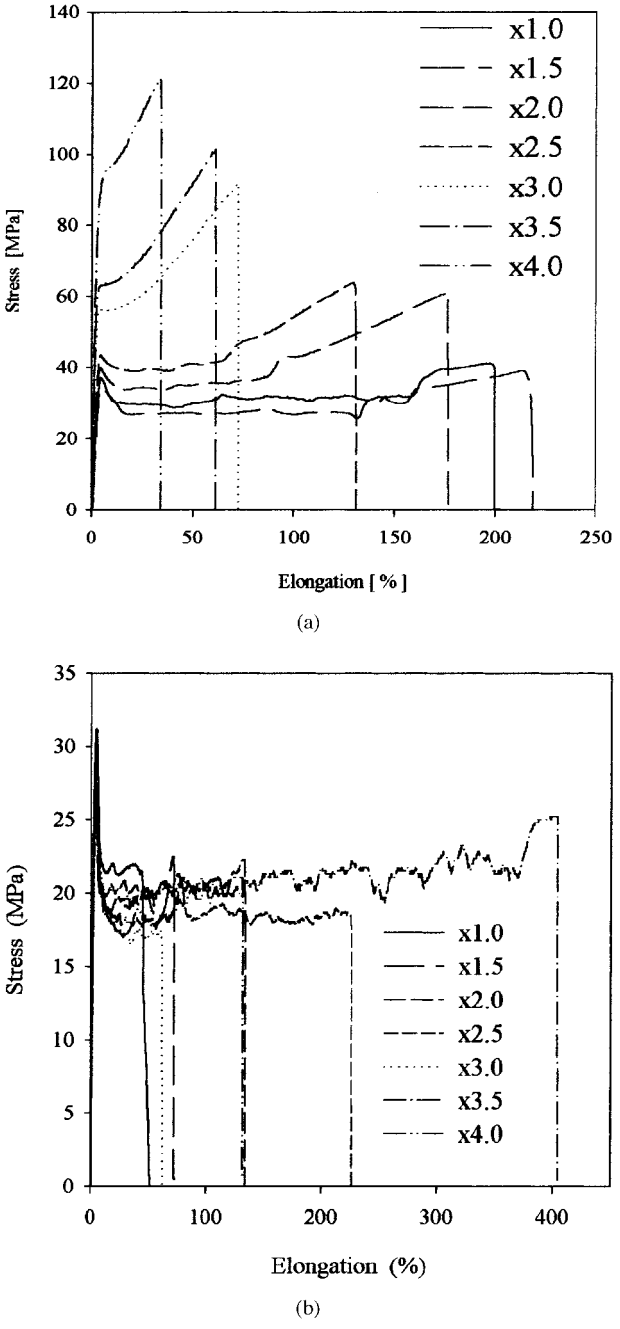

Figure 8 Typical mechanical stress–strain curves for non-oriented and oriented films of a 75%/25%/4 pph R-PET/R-HDPE/EGMA blend tested along (a) the machine direction and (b) the transverse direction.

plastic deformation for such a film along the machine direction started at a stress level of 62 MPa, which was followed by a very short plastic flow and longer strain hardening with the break above 100 MPa at a strain of more than 60%. A film with a draw ratio of 4 deformed up to 40% and fractured at 120 MPa.

The films that deformed in the transverse direction did not exhibit a stress increase with an increase in the draw ratio [see Fig. 8(b)]; the yield stress was around 30–32 MPa and was independent of the draw ratio. The strain at break varied greatly from sample to sample, but there was no correlation with the draw ratio. For example, some of the samples drawn to a draw ratio of 4.0 showed 400% deformation before the break. Such behavior of the films in the transverse direction followed from the fact that the film was not oriented in that direction during drawing in a plane-strain manner, and the capacity for high plastic deformation at a low stress was preserved.

Unoriented and oriented films were subjected to thermoforming in a standard machine. The formed shapes made from unoriented films and from films with a draw ratio above 2.5 were uniform, without excessive thinning of walls. The welding of films by a hot wire method proved to be simple and trouble-free.

CONCLUSIONS

The addition of a compatibilizer effectively changes the morphology of a blend. A dispersed phase forms smaller inclusions with better adhesion to the matrix.

There is an optimum content of the compatibilizer above which the improvement of mechanical properties is not significant. For the PET/HDPE blends compatibilized by EGMA, we found this optimum to be around 4 pph.

The film extrusion and orientation of an R-PET/R-HDPE/EGMA optimized blend in the production plant were smooth and trouble-free.

The crystalline phase of PET in oriented films assumed a strong texture resulting from the plane-strain state of deformation. The X-ray pole figures indicated the formation of a texture produced during stretching: the macromolecular chains in the crystals were increasingly oriented along the drawing direction, being stronger with an increasing draw ratio. Normals to (100) planes weakly clustered in the direction around the normal to the film plane for low draw ratios and became more pronounced when the draw ratio reached 2.5. For higher draw ratios, a new population of crystals appeared that concentrated with (100) normals oriented in the transverse direction. The normals to the (010) planes of the crystals were concentrated at first in two distinct populations tilted at some acute angles in the equatorial plane with respect to the flat film surface. With an increasing draw ratio, the additional fraction of crystals seen in the (100) pole figures was located with (010) normals perpendicular to the film surface. Because the initial unoriented material was nearly amorphous, the origin of the texture was mostly the strain-induced crystallization and to a lesser extent the plastic deformation and rotation of newly formed crystals.

There was a significant trace of anisotropic packing of chains in the amorphous phase in the plane perpendicular to the drawing direction. The orientation of the normals to the (100) close-packing plane suggested

that the chain segments in the amorphous phase were oriented along the machine direction. The splitting of the clustering of (100) normals in the equatorial zone was apparently caused by the pseudohexagonal packing of chain fragments in the amorphous phase of PET, being in register over the whole sample. The observation of pseudohexagonal packing of the oriented amorphous phase in PET was new and very important because it resolved the old dispute about how the oriented amorphous phase was arranged. The PET amorphous phase exhibited anisotropy: the glass transition occurred at different temperatures when the film was bent in different directions. The source of the anisotropy in the glass transition was the anisotropy of the amorphous phase: the pseudohexagonal packing and orientation of chain segments. It was evident that the free volume and frozen fraction of the amorphous phase exhibited some degree of anisotropy. A similar feature for the amorphous phase packing was observed previously in polypropylene deformed by plane-strain compression by rolling with side constraints.[27] Also, the main deformation mode here was plane strain; the geometry of plane-strain tension was enforced by the lateral friction of the film against the system of stretching rolls.

The nonoriented and oriented films obtained on the industrial machinery showed good mechanical properties, with strengths up to 120 MPa and elongations to break of 40% in the machine direction, whereas the mechanical properties in the transverse direction remained independent of the draw ratio and were similar to those for unoriented films.

Impurities present in the recycled components did not show any detrimental effect on the properties of the films; apparently, the admixtures of other polyolefins were also compatibilized with PET via a reaction with EGMA. Pigments and fillers present initially in R-HDPE were now evenly distributed over the film, leading to nontransparency and a gray-green appearance.

The anticipated application of these films is in the packing of technical goods as these films are easily thermoformed and welded.

References

1. Goracy, K.; Bledzki, A. TEMPUS Project 0644 Report on Recycling of Plastics; Kassel-Szczecin: 1995.
2. European Plastics News, Nov 2000, p 18.
3. Pawlak, A.; Pluta, M.; Morawiec, J.; Galeski, A.; Pracella, M. Eur Polym J 2000, 36, 1875.
4. Schiers, J. Polymer Recycling—Science, Technology and Applications; Wiley: Chichester, England, 1998; p 121.
5. Xanthos, M.; Dagli, S. S. Polym Eng Sci 1991, 31, 929.
6. Xanthos, M. Reactive Extrusion, Principles and Practice; Hanser: Munich, 1992.
7. Subramanian, P. M.; Mehra, V. Polym Eng Sci 1987, 27, 663.
8. Sambaru, P.; Jabarin, S. A. Polym Eng Sci 1993, 33, 827.
9. Carte, T. L.; Moet, A. J Appl Polym Sci 1993, 48, 611.
10. Akkapeddi, M. K.; Van Buskirk, B.; Swamikannu, X. Am Chem Soc Polym Mater Sci Eng 1992, 67, 317.
11. Dagli, S. S.; Kamdar, K. M. Polym Eng Sci 1994, 34, 1709.
12. Akkapeddi, M. K.; Van Buskirk, B.; Mason, C. D.; Chang, S. S.; Swamikannu, X. Polym Eng Sci 1995, 35, 72.
13. Kalfglou, N. K.; Skafidas, D. S.; Kallistis, J. K.; Lambert, J. C.; Van der Stappen, L. Polymer 1995, 36, 4453.
14. Pietrasanta, Y.; Robin, J.-J.; Torres, N.; Boutevin, B. Macromol Chem Phys 1999, 200, 142.
15. Xanthos, A.; Patel, A.; Dey, S.; Dagli, S. S.; Jacob, C.; Nosker, T. J.; Renfree, R. W. Adv Polym Technol 1994, 13, 231.
16. Pazzagli, F.; Pracella, M. Macromol Symp 2000, 149, 225.
17. Pawlak, A.; Morawiec, J.; Pracella, M.; Pazzagli, F.; Galeski, A. J Appl Polym Sci 2002.
18. Bartczak, Z.; Galeski, A.; Pluta, M. J Appl Polym Sci 2000, 76, 1746.
19. Daubeny, R. P.; Bunn, C. W.; Brown, J. C. Proc R Soc London Ser A 1954, 226, 531.
20. Pracella, M.; Galeski, A.; Kummerloewe, C.; Lednicky, F. Recycling of Unsegregated Scrap Plastics by Compatibilized Blending; EC Copernicus Project Final Report 2000; p 17.
21. Faisant de Champchesnel, J. B.; Bower, D. I.; Ward, I. M.; Tassin, J. F.; Lorentz, G. Polymer 1993, 34, 3763.
22. Lapersonne, P.; Tassin, J.; Monnerie, L. Polymer 1991, 32, 3331.
23. Galeski, A.; Argon, A. S.; Cohen, R. E. Macromolecules 1991, 24, 3945.
24. Galeski, A.; Bartczak, Z.; Argon, A. S.; Cohen, R. E. Macromolecules 1992, 25, 5707.
25. Bartczak, Z.; Galeski, A.; Argon, A. S.; Cohen, R. E. Polymer 1996, 37, 2113.
26. Bellaire, A.; Argon, A. S.; Cohen, R. E. Polymer 1993, 34, 1393.
27. Morawiec, J.; Bartczak, Z.; Kazmierczak, T.; Galeski, A. Mater Sci Eng A 2001, 317, 21.
28. Morawiec, J.; Bartczak, Z.; Pluta, M.; Galeski, A. J Appl Polym Sci 2002.